Applied Catalysis B: Environmental 208 (2017) 135–147

Contents lists available at ScienceDirect

Applied Catalysis B: Environmental

journal homepage: www.elsevier.com/locate/apcatb

Insight into the catalyst/photocatalyst microstructure presenting the same composition but leading to a variance in bacterial reduction under indoor visible light

Sami Rtimi[a,**], Cesar Pulgarin[a], Martin Robyr[b], Arseniy Aybush[c], Ivan Shelaev[c], Fedor Gostev[c], Victor Nadtochenko[c,d,e], John Kiwi[a,*]

[a] Ecole Polytechnique Fédérale de Lausanne, EPFL-SB-ISIC-GPAO, Station 6, CH-1015 Lausanne, Switzerland
[b] Institute of Earth Sciences, University of Lausanne, Building Geopolis, UNIL, CH-1015, Lausanne, Switzerland
[c] N. N. Semenov Institute of Chemical Physics, Russian Academy of Sciences, Kosygina 4, 119991 Moscow, Russia
[d] Institute of Problem of Chemical Physics Russian Academy of Sciences, Semenov Av1, Chernogolovka, 142432, Russia
[e] Moscow State University, Faculty of Chemistry, Moscow 119991, Russia

ARTICLE INFO

Article history:
Received 16 December 2016
Received in revised form 10 February 2017
Accepted 11 February 2017
Available online 17 February 2017

Keywords:
$CuOx-TiO_2$
Microstructure
CuOx mapping
Transients
E. coli
XPS

ABSTRACT

Insight into two different uniform atomic-scale microstructures of Cu- and Ti-oxides sputtered on polyethylene (PET) presenting different *redox* properties and a distinct bacterial inactivation dynamics. Co-sputtered ($CuOx-TiO_2$-PET) consists mainly of CuO. It leads to bacterial inactivation kinetics within 20 min under very low intensity actinic light (0.5 mW/cm^2). The sequential sputtered ($CuOx/TiO_2$-PET) consist mainly of Cu_2O and led to bacterial inactivation within 90 min. Evidence for *redox* catalysis is present leading to bacterial inactivation by X-ray photoelectron spectroscopy (XPS). The Cu and Ti uniform distribution on the catalyst surface was mapped along the coating thickness by wavelength dispersive spectrometry (WDS). The inactivation time of *E. coli* determined by fluorescence stereomicroscopy was in agreement with the time found by agar plating. The short-lived transient intermediates on the co-sputtered catalyst were followed by laser spectroscopy in the femto/picosecond region (fs-ps). By atomic force microscopy (AFM) the roughness of the co-sputtered (CuO) and sequentially sputtered samples (Cu_2O) were found respectively as 1.63 nm and 22.92 nm. The magnitude of the roughness was correlated with the bacterial inactivation times for both types of catalysts. The differentiated mechanisms for the vectorial charge transfer on co-sputtered and sequential sputtered $CuOx/TiO_2$catalysts and it is suggested as one of the factors leading to a distinct bacterial inactivation kinetics.

1. Introduction

The search of innovative antibacterial materials/surfaces able to inactivate bacteria/pathogens within very short times presenting high stability, adhesion and long-operational lifetime has gained in attention during the last decade due to the increase in the number of pathogenic infections leading to serious illness and death [1–5]. Biofilms spreading bacteria in hospitals, schools, public places are the most common and dangerous form of infection by bacteria, fungi and viruses. These pathogens are capable of living in environments under minimal life conditions developing films adhering to the surfaces. These surfaces spread bacteria continuously into the environment. Biofilm formation is at the origin of 80% of all microbial infections making biofilms a primary health concern [6]. What makes the problem even more complicated is that bacteria embedded in a biofilm can survive concentrations of antiseptic/antibiotics several times higher than the concentration required to kill planktonic cells of the same species [7]. Healthcare- facilities associated infections (HCAI's) are becoming a worldwide problem. Multidrug resistant bacteria to antibiotics are not available or are ineffective in the case of several infections leading to patient death. Prolonged antibiotic application times make pathogens resistant to its initial abatement effect [8–10].

TiO_2, Cu and TiO_2/Cu work addressed bacterial inactivation by colloidal suspensions and films prepared by sol-gel methods leading to films effective in bacterial inactivation under UV-light [11–13]. More recently, Qiu et al. reported Cu/TiO_2 powdwes inducing self-cleaning of dyes besides *E. coli* bacterial inactivation [14].

* Corresponding author.
** Corresponding author. Tel.: +41216936150.
E-mail addresses: sami.rtimi@epfl.ch (S. Rtimi), john.kiwi@epfl.ch (J. Kiwi).

http://dx.doi.org/10.1016/j.apcatb.2017.02.043
0926-3373/

To obtain a better film adhesion/reproducibility on the underlying support and preparation reproducibility of these antibacterial films compared to colloidal deposited films, sputtering of Cu, TiO_2 or both on glass have been reported [15–17].

The bacterial inactivation of TiO_2 and TiO_2/Cu-doped under solar actinic light has been the objective of the work reported by some laboratories during the last years. Recent results have reported by Pillai et al. [18–20], Espirito-Santo et al. [21,22], Borkow et al. [23,24], Liu et al. [25], Dionysiou et al. [26,27] and Bahneman et al. [28] for disinfection on surfaces energized by solar irradiation. Because of its unique electronic structure, magnetic and optical properties, Cu_2O has been used in catalysis/photocatalysis [29] and in solar energy conversion into electrical energy [30–32]. Films made-up by Cu and Cu-TiO_2 co-sputtered or sequential sputtered have been reported by our laboratory during the last few years [33–37]. Surface modifications of TiO_2 films incorporating Ag in the dark and under light as antibacterial agent have been widely reported by Cushnie et al. [38] and Dias [39]. The present work provides insight correlating the atomic-scale microstructure/redox properties and their effect on the bacterial inactivation kinetics. If an acceptable kinetics, stability and bacterial inactivation efficiency be attained by composite bactericide surfaces, solar light could be put to work for antibacterial purposes

This study addresses Cu/TiO_2 surfaces for two reasons: a) Cu is more cytotoxic per unit weight compared to Ag. This enables extremely low amounts on the ppb–range of Cu to be used to inactivate bacteria and b) the lower cost of Cu compared to the noble silver metal. This study reports on innovative CuOx-TiO_2 sputtered on polyethylene terephthalate (PET) with a similar composition but a distinct atomic scale microstructure leading to a different *E. coli* bacterial inactivation kinetics. Identification of the transients by femtosecond pulses was carried out for transients induced by laser pulses 375 nm within the 380–800 nm spectral region This study presents the first evidence mapping the distribution of the Cu and Ti nanoparticles on the film surface by wavelength dispersive spectrometry (WDS). This allows the correlation of the surface microstructure and the bacterial inactivation kinetics for the two composite catalysts investigated during the course of this preventing biofilm formation.

2. Experimental, materials and methods

2.1. Plasma pretreatment, sputtering details and catalyst loading determination

PET fabrics were RF-plasma pretreated in the following way: The polyethylene terephthalate (PET) fabrics were pretreated in the cavity of the RF-plasma unit (Harrick Corp. 13.56 MHz, 100 W) at a pressure of ~1 Torr. The topmost PET-layers of 2 nm (~10 atomic layers) were RF-plasma pretreated for 15 min. This pretreatment modifies the PET surface by: a) etching the PET surface due to the residual O-radicals still present in the gas of the RF-plasma chamber at ~1 Torr, b) introducing hydrophilic groups on the PET-surface and c) breaking the intermolecular PET H—H bonds leading to a partial segmentation of PET. TiO_2 and CuOx exchanged on the PET-surface then bind the PET-oxidative sites by electrostatic attraction and chelation/complexation [40]. Pre-treated samples were subsequently sputtered from a Cu and a Ti 5 cm diameter targets (Kurt Lesker, East Sussex, UK) by direct current magnetron sputtering (DCMS) in an O_2 gas flow (5%) on the PET substrate. The residual pressure P_r in the sputtering chamber was adjusted to P_r 10^{-4} Pa. The substrate to target distance was set at 10 cm. The polyethylene (PET) used as substrate was made up by highly branched low crystalline semi-transparent film with the formula $H(CH_2—CH_2)_nH$. The (LDPE) 0.1 mm thick was obtained from Goodfellow, UK (ET3112019), had a density of 0.92 g/cm^3, and a flowing point of 185 °C.

Table 1
XRF determination of Ti and Cu loading on Co-sputtered and sequentially sputtered samples on PET.

	Wt% TiO_2/wt PE	Wt% Cu/wt PE
TiO_2-Cu co-sputtered for 3 min	0.11	0.08
TiO_2/Cu sequentially sputtered for 8 min/40 s	0.14	0.05

2.2. X-ray fluorescence (XRF), atomic force microscopy (AFM) and sample diffuse reflectance spectroscopy (DRS)

The Cu and Ti-content on the PET film was evaluated by X-ray fluorescence (XRF) in a PANalytical PW2400 spectrometer. The results are presented in Table 1. The AFM scanning head was from SMENA-A, NT-MDT, Moscow provided for with a silicon probe (NSG01, NT-MDT) and operated in an intermittent contact mode. The AFM head was also provided for with a scanning research microscope (Olympus IX71, Japan). The scan areas selected to record the sample topography were 3×3 microns by way of 1024×1024 pixels. The local height was recorded after each scan and used to build the sample topography in the x,y coordinates. Diffuse reflectance spectroscopy was carried out in a Perkin Elmer Lambda 900 UV–vis-NIR spectrometer provided for with a PELA-1000 accessory within the wavelength range of 200–800 nm and a resolution of one nm. X-ray fluorescence (XRF) of the sputtered samples was performed.

2.3. Bacterial inactivation kinetics and inductively coupled plasma mass spectrometry (ICP-MS)

The evaluation of the bacterial inactivation of *E. coli* was carried out by plate counting agar method. The sample of *Escherichia coli* (*E. coli* K12) was obtained from the Deutsche Sammlung von Mikro-organismen und Zellkulturen GmbH (DSMZ), Braunschweig, Germany to test the sample bacterial reduction activity. The sputtered PET-films were sterilized keeping them at 70 °C overnight. Aliquots of 50 μL bacterial culture suspended in NaCl/KCl (8 g/l NaCl and 0.8 g/l KCl) solution with a concentration of 4×10^6 CFU mL^{-1} were placed on sputtered and unsputtered PET control samples. The samples were placed on Petri dishes provided with a lid to prevent evaporation. At preselected times, the samples were transferred into a sterile 2 mL Eppendorf tube containing 950-μL autoclaved NaCl/KCl saline solution. These solutions were subsequently mixed thoroughly using a Vortex for 3 min. Serial dilutions were made in NaCl/KCl solution taking 100 μL aliquots. Then 100 μL aliquots were pipetted onto a nutrient agar plate, for the bacterial counting by the standard plate method. These agar plates were incubated, lid down, at 37 °C for 24 h before the colonies counting. Triplicate runs were carried for the bacterial CFU mL^{-1} determination reported in this study. To verify that no re-growth of *E. coli* occurs after the first bacterial reduction cycle, the nanoparticle film was incubated again on an agar Petri dish at 37 °C for 24 h.

A FinniganTM ICP-MS instrument was used was to assess the ions release after the sample washing in MQ-water and vortexed for 2 min. ICP-MS is equipped with a double focusing reverse geometry mass spectrometer with an extremely low background signal and a high ion-transmission coefficient.

2.4. Sample wavelength dispersive spectrometry (WDS)

The spatial distribution of Cu and Ti was imaged by wavelength dispersive spectrometry (WDS) using an electron probe

MicroAnalyze-JEOL 8200. The instrument was operated at 25 kV with a current of 15 nA and a focused beam. The compositional mapping of an area of 1024 × 1024 pixels was carried out at 50 ms per pixel. The two films composed of Cu and Ti on a glass section were subjected to microprobe analysis in order to image the spatial distribution of these two elements. A slight decrease of the current or a slight defocusing of the beam was observed within the acquisition time. X-rays are generated randomly within the excitation volume of each sample and the number of X-ray detected (intensity) was subject to statistical fluctuation. These fluctuations follow a Gaussian distribution defining the standard deviation $\sigma = N^{0.5}$.

2.5. Femtosecond laser spectroscopy

The Supplemental material S1 shows the set-up of the femtosecond pump laser unit and detection system [41,43]. The output of a Ti sapphire oscillator (800 nm, 80 MHz, 80 fs, "Tsunami", "Spectra-Physics", USA) was amplified by a regenerative amplifier system ("Spitfire", "Spectra-Physics", USA) at the repetition rate of 1 KHz. The Gauss pulse was tuned at 25 fs at 545 nm. The second beam was focused onto a thin quartz cell with H_2O to generate super-continuum probe pulses. The pulses were then attenuated, recombined, and focused onto the sample cell. The pump and probe light spots had diameters of 300 and 120 μm, respectively. The pump pulse energy was attenuated to 500 nJ to optimize the light excitation. The laser pulse frequency was adjusted by way of a control amplifier SDG II Spitfire 9132 manufactured by Spectra-physics (USA). The pulse operation frequency was 50 Hz, which is sufficiently low to exclude permanent bleaching of the sample. The circulation rate in the flow cell was fast enough to avoid multiple excitations in the sample volume. The relative polarizations of pump and probe beams were adjusted to 54.7° (magic angle) in parallel and perpendicular polarizations. The super continuum signal out of the sample was dispersed by a polychromator ("Acton SP-300") and detected by CCD camera ("Roper Scientific SPEC-10"). Transient absorption spectral changes ΔA (t, λ) were recorded within the range of 380–800 nm Control experiments were carried out for non-resonant signals of coherent spike from net PE film.

2.6. Fluorescence stereomicroscopy of the loss of bacterial viability

Fluorescence stereomicroscopy was carried out on samples inoculated with *E. coli* and incubated in a humidifier. A fluorchrome dye is used as staining agent received from Filmtracer™ Live/Dead Biofilm Viability Kit from Molecular Probes, Invitrogem Co. The kit contains dyes to stain differentially living and dead cells. The fluorescence of the samples was monitored in a Leica MZ16FA GmbH

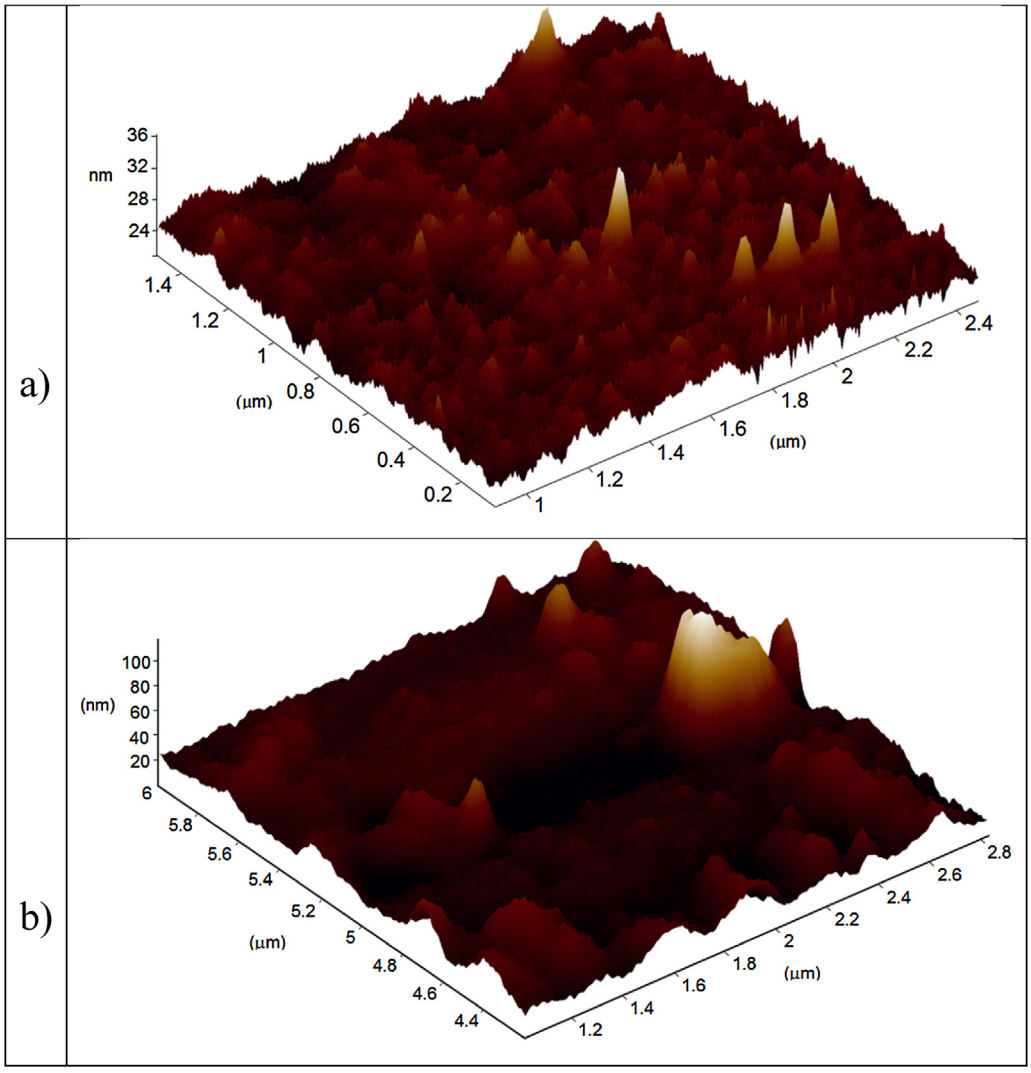

Fig. 1. AFM imaging of: (a) sequentially sputtered CuOx/TiO_2-PET and (b) co-sputtered CuOx-TiO_2-PET.

Wetzlar fluorescence stereomicroscope unit and the images were processed using the LAS vq.7.0 software. Adhesion of the bacteria (6×10^8 CFU mL^{-1}) to the samples was allowed for 2 min prior to the washing of the samples to remove the non-adherent bacteria.

2.7. Sample X-ray photoelectron spectroscopy (XPS)

The X-ray photoelectron spectroscopy (XPS) of the CuOx-TiO_2-PET films was measured using an AXIS NOVA photoelectron spectrometer (Kratos Analytical, Manchester, UK) provided for with monochromatic AlK_a (h ν = 1486.6 eV) anode. The carbon C1 s line with position at 284.6 eV was used as a reference to correct the charging effect. The surface atomic concentration was determined from peak areas using the known sensitivity factors for each element [44,45]. The spectrum background was subtracted according to Shirley [46]. The XPS spectral peaks were deconvoluted with a CasaXPS-Vision 2 program from Kratos Analytical UK.

3. Results and discussion

3.1. Surface characterization of co-sputtered and of the sequential sputtered samples

Fig. 1 shows the images obtained by atomic force microscopy (AFM) for the co-sputtered sample (CuOx-TiO_2-PET) and the sequential sputtered (CuOx/TiO_2-PET) sample. The scanned field shown in Fig. 1 allowed the estimation of the roughness (Rg) of the co-sputtered CuOx-TiO_2-PET of 22.92 nm and of the sequentially sputtered CuOx/TiO_2-PET of 1.63 nm. Roughness is a measure of the vertical deviations (valley and peaks) from an ideal flat surface. The CuOx-TiO_2-PET with an Rg value of 22.92 nm presents a high frequency of peaks at short distances between themselves. This gives raise to many points of contact with the *E. coli* ellipsoid 1 micron in size and the CuOx-TiO_2-PET surface. These contact points allow the transfer from the sample to the bacteria cell envelope leading to a fast bacterial inactivation (see Fig. 6). The sequentially sputtered CuOx/TiO_2-PET (1.63 nm) samples present contact points further apart from each other reducing the contact between the sample and the bacteria. This means a low number of catalytic points able to transfer charge to *E. coli*. The increase in roughness favoring the attachment of bacteria to several surfaces has been reported, but this observation cannot be extrapolated to surfaces directed towards the oxidation of pollutants [1,28].

The optical properties of the sputtered samples are shown in Fig. 2 by diffuse reflectance spectroscopy (DRS). Fig. 2, trace 1) shows the O2p electron transition to the Ti 3d-level. By indirect-band transition, the conduction band electrons (cbe-) recombine with the valence band (vbh+) in trapping states positioned at (−0.1/−0.2 eV). The optical absorption of the co-sputtered CuOx-TiO_2-PET in Fig. 2, trace 1) exhibits a long-tail absorption beyond the 400 nm, due to the 0.08%Cu/wt% in the sample (see Table 1). Next, Fig. 2, trace 2) notes the stronger optical transition with a significant red shift at the absorption edge of the CuOx/TiO_2-PET sample due to the absorption of the superimposed CuOx layers. The TiO_2-PET absorption in Fig. 2, trace 4) is seen <410 nm. Fig. 2, trace 3) shows the optical absorption spectrum of CuOx-PET. The optical absorption between 500 and 600 nm is due to the inter-band transition of Cu (I). The absorption between 600–720 nm is attributed to the exciton band and the Cu(II) d–d transition [40]. Due to the CuOx present in the co-sputtered/sequentially sputtered samples (Fig. 2, traces 1 and 2), the samples present trapping sites within their respective band-gap. This allows the TiO_2/CuOx samples to absorb visible light compared to the TiO_2 band-gap. The absorption shift to the red spectral region allows the TiO_2/CuOx sample to absorb visible light >400 nm (see Supplemental material S2).

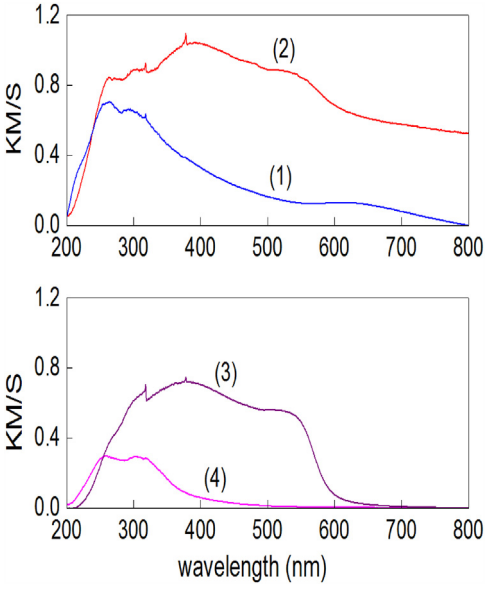

Fig. 2. Diffuse reflectance spectroscopy of samples: (1) CuOx-TiO_2-PET co-sputtered from one target for 3 min, (2) CuOx/TiO_2-PET sequentially sputtered for 8 min by Ti followed by Cu for 40s, (3) CuOx-PE sputtered for 40 s and (4) TiO_2-PET sputtered for 8 min.

3.2. Wavelength dispersive spectrometry analysis (WDS)

Fig. 3a shows the wavelength dispersive spectrometry mapping the Ti and Cu in the co-sputtered (CuOx-TiO_2-PET) sample. This sample presented a homogeneous distribution of both elements on the PET sample surface. The coating thickness was 476 ± 28 nm thick. The resulting maps for Cu and Ti on the co-sputtered and sequentially sputtered samples are presented in Figs. 3 and 4 and show the X-rays detected for Ti and Cu each 10 μ. Fig. 4a shows by WDS a homogenous Cu and Ti distribution on the PET-surface for the sequential sputtered CuOx/TiO_2-PET sample with a thickness 510 ± 30 nm. This film consists of two superposed thin layers made out by a Ti layer 380–400 nm thick and a second Cu-topmost layer of 110–130 nm. Fig. 3b and c shows the Cu and Ti uniform and homogeneous distribution in the co-sputtered sample for particles with sizes <0.1 μ. These nanoparticles aggregate with a different orientation/density and give raise to X-Ray Ti and Cu reflections giving rise to different colors in the same Fig. (3/4). This is shown in Figs. 3a and 4a for Ti and Cu respectively for co-sputtered and sequential sputtered samples.

The intensity of the WDS signals for Cu was similar equal for both samples. This is consistent with the data reported in Table 1, since the Cu percentage determined by X-ray fluorescence (XRF) was seen to be low but very close for both elements. The difference in intensity detected for Ti between the co-sputtered and the sequentially sputtered samples is readily understood since in the sequentially sputtered samples, Ti constitutes the underlayers of the film. As the generation of Ti characteristic X-rays, the co-sputtered sample will generate a larger amount of Ti X-rays compared to the sequential sputtered samples. The X-ray maps for Cu in the sequential and co-sputtered samples show a slight decrease of the Cu X-ray intensity toward the right side of the mapped areas in Figs. 3a and 4a. The excitation volume generated at 25 kV within the sample is larger than the thickness of the film. This leads to a slight variation in the film thickness, surface roughness and X-ray generation.

For the co-sputtered and sequential sputtered samples, the number of X-ray (N) of Cu detected by second is ca.1995 with a standard deviation σ = 44,5 and 1940 with σ = 44 respectively. Con-

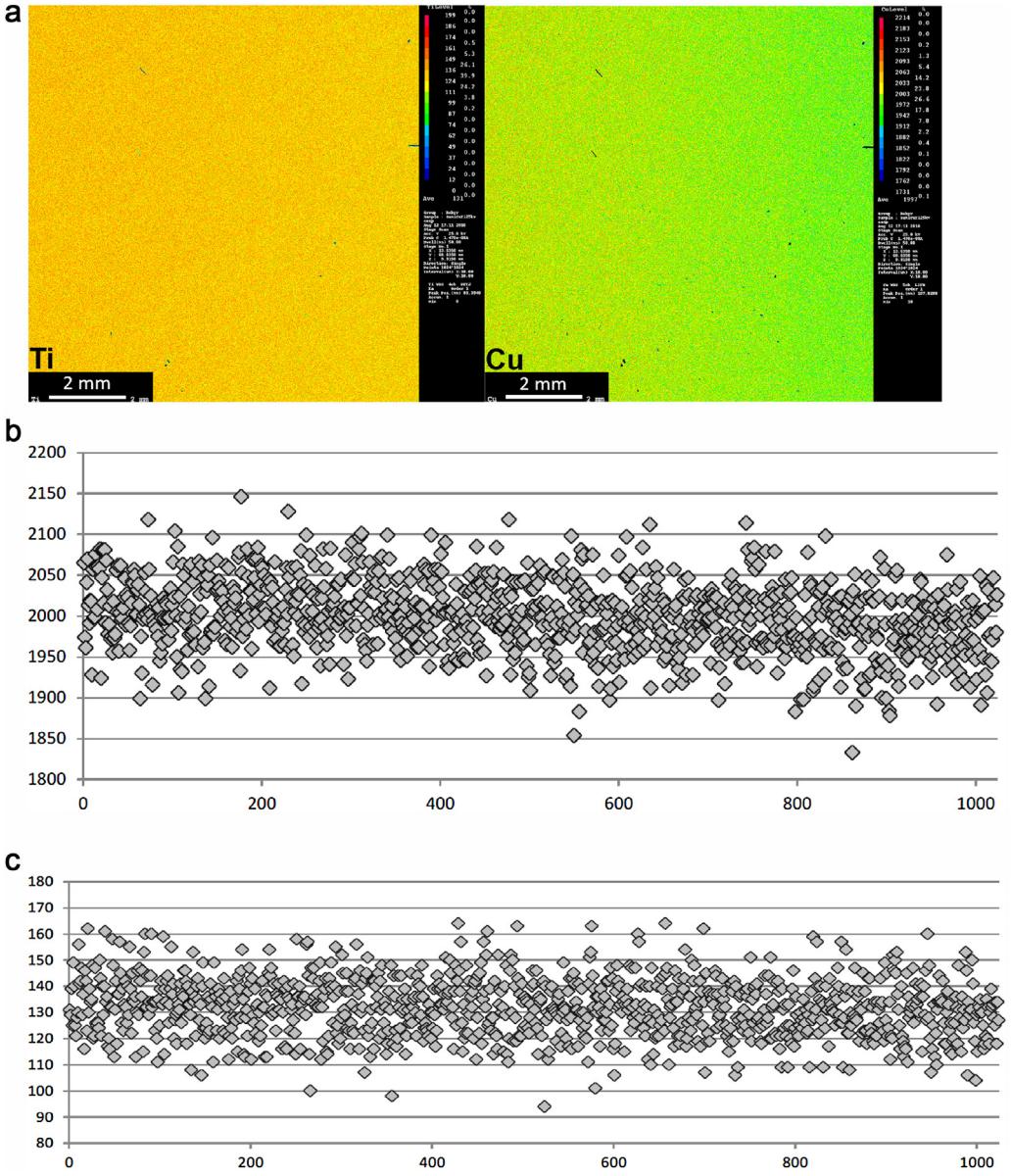

Fig. 3. a. Wavelength dispersive spectrometry (WDS) mapping of Ti and Cu of a CuOx-TiO_2-PET (3 min) co-sputtered sample. b. Wavelength dispersive spectrometry (WDS) mapping of Cu in the CuOx-TiO_2-PET (3 min) co-sputtered sample. c. Wavelength dispersive spectrometry (WDS) mapping of Ti in the 3 min CuOx-TiO_2-PET co-sputtered sample.

sidering a standard deviation at 2σ, the probability that a new single measurement of Cu will lie within 1995 ± 89 counts for the co-sputtered sample and 1940 ± 88 counts for the sequentially sputtered sample is 95% a limit values for homogeneity. In both samples, even if the intensity of Cu shows a slight decrease, the mean values remain within the uncertainties domain. The spatial distribution of Cu in these samples can be considered as homogeneous.

3.3. Femtosecond spectroscopy of co-sputtered transients

For the study of solid-phase redox reactions, the electron mobility, the electronic relaxation times, transient absorption intensity (T-A) and excided states relaxation times in the fs to the ms range, has been a way to clarify the charge transfer to the acceptor states in the short time scale [47,48]. Femtosecond pump-probe spectroscopy has been used in this study since it is a powerful technology to follow ultrafast processes [49]. Short tine laser spectroscopy has been used to monitor the transients/electron injection dynamics in solid surfaces in a similar way as it has been carried out in this study [50,51]. Bleaching and e-/h+ recombination rates have been reported for by fast kinetics for allowed charge-transfer in hetero-junctions and sensitized processes in semiconductors [52,53].

Excitation by 375 nm can produce e−/h+ pairs in TiO_2 and CuOx in parallel with the formation of CuOx excitons. Femtosecond transient spectra shows in Fig. 5a predominantly the signal for CuOx. Signals for TiO_2 in the spectral region 400–750 nm were mainly due to absorption of the cbe-. A strong negative absorbance was detected in the 400–450 nm in Fig. 5a due to: a) the bleaching (BL) due to the depletion of the ground state cbe− (g.s), b) the bleaching BL-bands due to the Kerr shift of the absorption band-edge [42] and c) the CuOx stimulated emission (SE) originating from light induced CuOx excitons generated when a photon hits the CuOx-

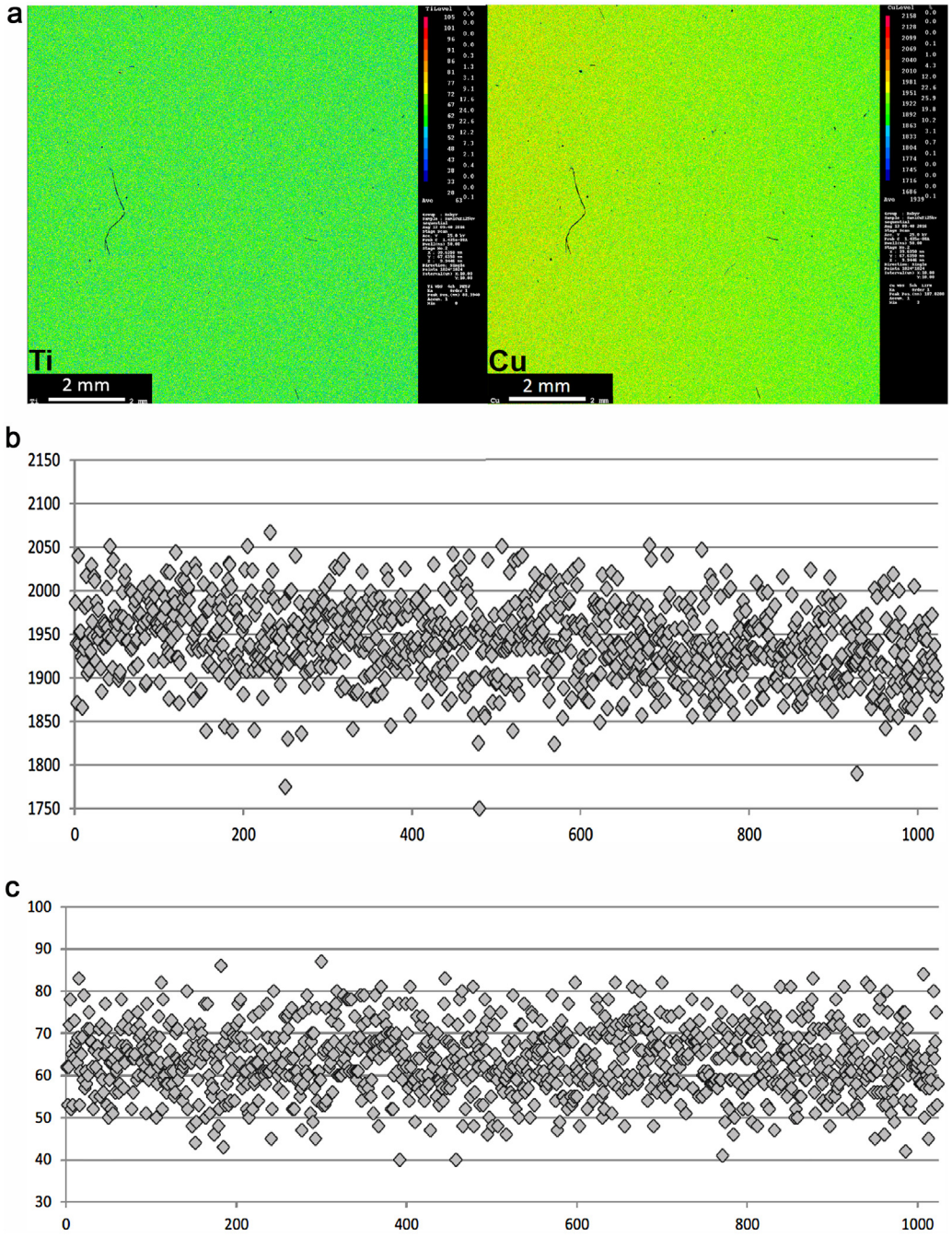

Fig. 4. a. Wavelength dispersive spectrometry (WDS) mapping of Ti and Cu in a sample (CuOx/TiO_2-PET) sample sputtered for 8 min (Ti) followed by Cu sputtered sequentially for 40s. b. Wavelength dispersive spectrometry (WDS) mapping of Cu sputtered for 40 s for a sequential sputtered CuOx/TiO_2-PET sample. c. Wavelength dispersive dpectrometry (WDS) mapping of Ti sputtered for 8 min in a sequential sputtered CuOx/TiO_2-PET sample.

TiO_2-PET surface producing a bound electron. This exciton travels in a particle-like fashion through the sample lattice without net transfer of charge. The negative absorption observed in Fig. 5a above 620 nm was due to CuOx excitons. Disappearance of the SE 400–450 nm correlates in Fig. 5a with the SE signals >620 nm. At time delays <300 fs, the coherent wave-packets give rise to the oscillations observed in the transients beyond 620 nm in Fig. 5a.

Upon photo-excitation at 375 nm, Fig. 5b shows the decay of different species at different wavelength in the visible range. Fig. 5b shows that the femtosecond laser pulse does not generate a well-defined single transient that could be fitted by a single exponential. Neither a double exponential (Kohlrausch's stretched exponential fitting) could fit the transients induced by the femtosecond pulse [43]. The decay of a species at 710 nm proves the presence of excited states in the red spectral region. This is important in relation to the absorption of the light from the actinic light source with an emission up to 720 nm. Fig. 5c shows that the 375 nm femtosecond laser pulse induce three main transient species. The assignment of the transient kinetic species K1, K2 and K3 is shown in the right hand side in Fig. 5c. The unambiguous assignment of the species associated with each the decay is not possible with the available spectroscopic information. Fig. 5c shows that transients exist in the fs time scale <500 fs, in the ps time scale 0.5–10 ps and in the time scale 10–500 ps.

3.4. Bacterial inactivation kinetics in the dark and under light irradiation determination of the ions eluted within the bacterial inactivation runs

The fast bacterial inactivation within 20 min for *E. coli* is readily seen in Fig. 6, trace 1) for the co-sputtered CuOx-TiO_2-PET. Fig. 6, trace 2) shows that a sample sputtered for 2 min did not have enough Cu to induce a rapid kinetics as it was the case for the 3 min sputtered sample shown in Fig. 6, trace 1trace 1). Samples shown by traces 3) and 4) sputtered for 5 and 10 min respectively, induced a slower bacterial inactivation kinetics due to: a) the agglomeration

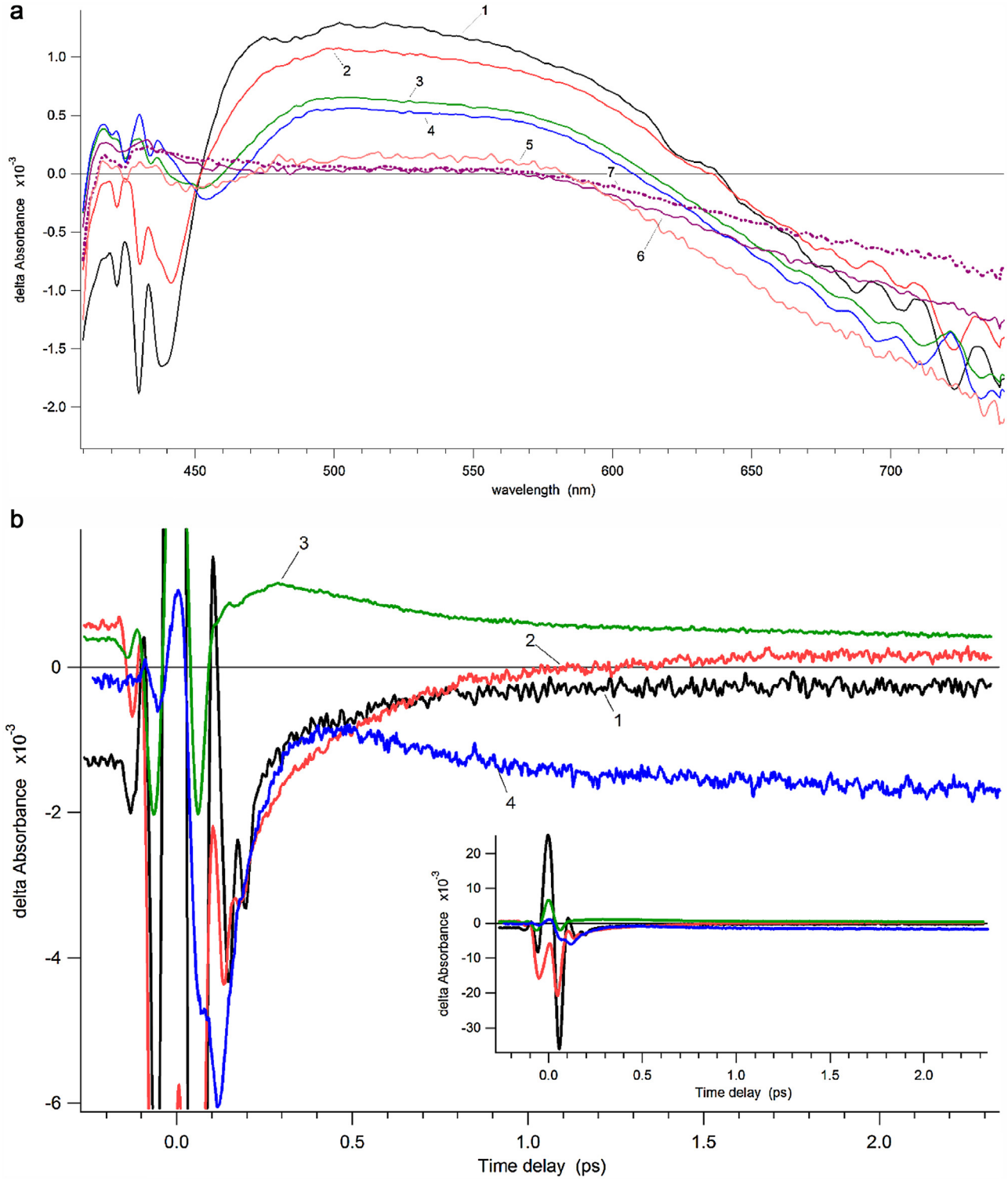

Fig. 5. a. Transient spectra of the sample measured at the magic angle of 54.7° between the polarization of pump and probe pulses (under the condition that the rotation of the polarization does not emit signals in the transient absorption region). Pulse at 375 nm, pulse energy 300 nJ, pulse duration 50 fs. Time delays: 1) 300 fs, 2) 500 fs, 3) 1.1 ps, 4) 1.9 p, 5) 9 ps, 6) 270 ps, 7) 500 ps. b. Transient kinetics of the co-sputtered CuOx-TiO_2-PET (3 min) sample registering for the decay of different species photo-excited by a 375 nm femtosecond pulse (as in Fig. 6a) showing the decay of transients at wavelengths: 1) 410 nm, 2) 440 nm, 3) 550 nm and 4) 710 nm. c. S1, S2 and S3: traces for the main transient species induced by the 375 nm femtosecond pulse as a function of the wavelength. K1, K2 and K3 show the decay of the transient species shown in S1, S2 and S3.

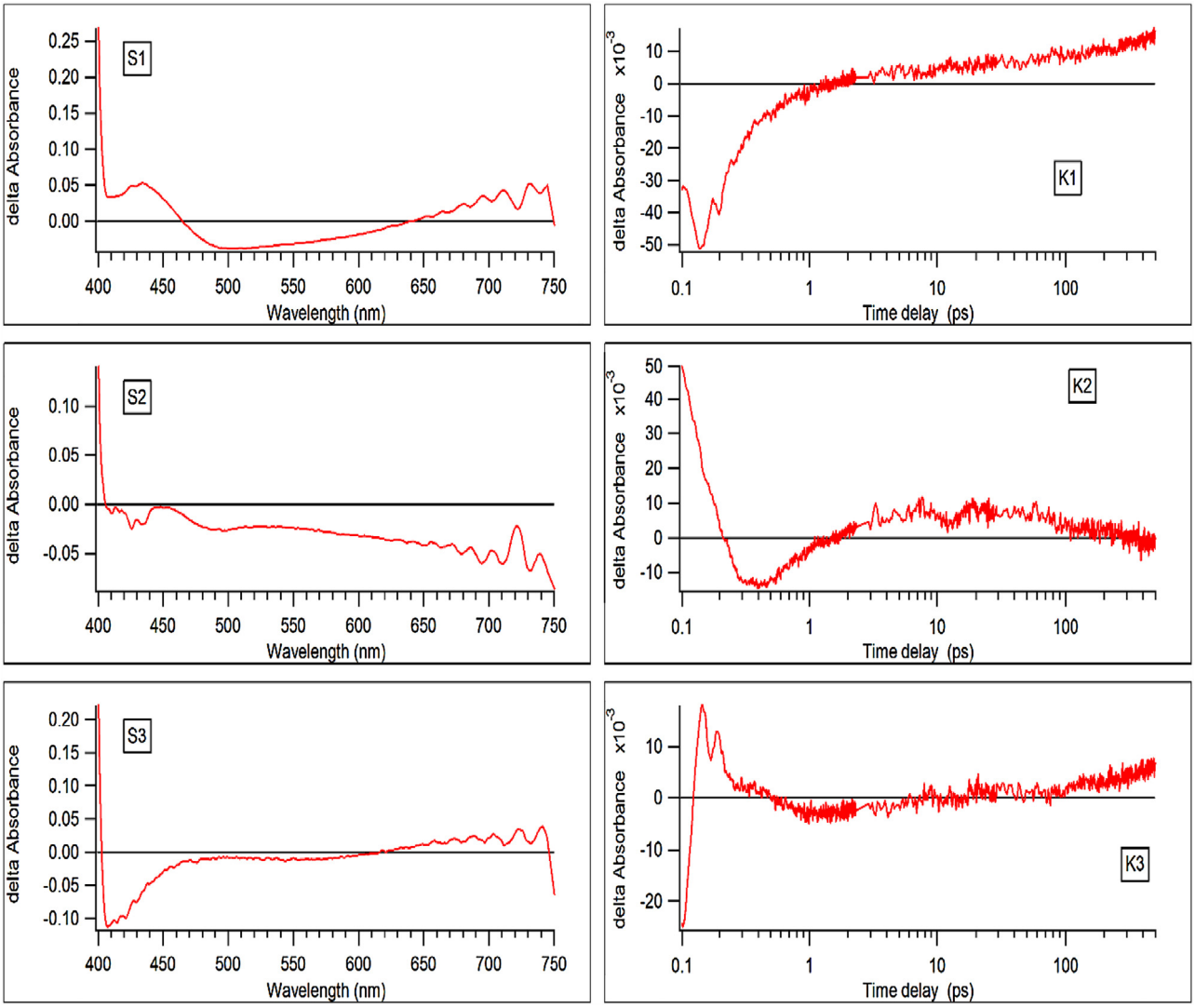

Fig. 5. (*Continued*)

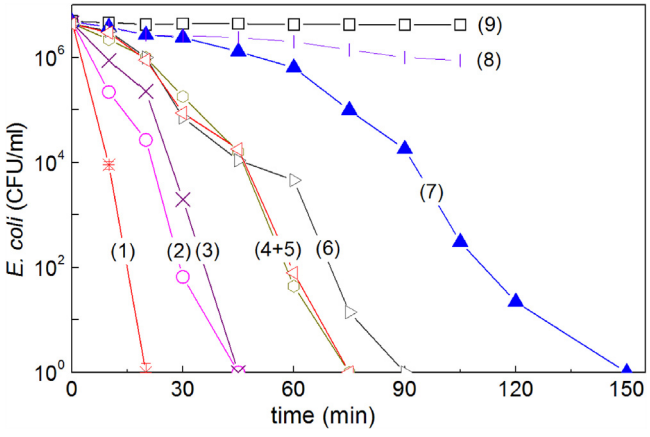

Fig. 6. Bacterial inactivation under 0.5 mW/cm^2 indoor actinic light (Philips Master TLD-18W/865) mediated by co-sputtered CuOx-TiO_2-PET for: (1) 3 min, (2) 2 min, (3) 5 min, (4) 10 min, (5) CuOx/TiO_2 sequentially sputtered for 8 min/40s, (6) Cu sputtered alone for 2 min,(7) TiO_2-Cu co-sputtered for 3 min in the dark, (8) TiO_2-PET sputtered for 8 min and (9) uncoated PET under light.

of Cu in bigger particles with less catalytic sites/unit mass, b) the longer path the Cu-ions have to cross on larger Cu-particles/films before reaching the *E. coli* LPS-envelope and c) the slower diffusion of the Cu-charges occurring on thicker Cu-layers [54]. The *E. coli* K-12 is 1 μ in size (see pertinent information in the experimental section) [55] allowing for contact sites between the Cu and Ti nanoparticles and the bacteria. These contact points direct the electron/hole injection generated in the CuOx-TiO_2-PET in contact with the *E. coli* 7–8 nm thick lipopolysaccharide (LPS) double-layer and the 2–3 nm thick peptidoglycan layer.

The slower bacterial inactivation induced by the sequential CuOx/TiO_2-PET is shown in Fig. 6, trace 5. This shows that the microstructure of Cu and Ti play a significant role in the bacterial inactivation kinetics. Cu-sputtered samples by themselves inactivate bacteria under light irradiation within 90 min (Fig. 6, trace 6). This time is five times longer compared to the inactivation time required by the CuOx-TiO_2-PET samples (Fig. 6, trace 1). This shows the synergy occurring between TiO_2 and Cu. Fig. 6, trace 7) reports the co-sputtered sample inducing bacterial inactivation in the dark. Samples are therefore in bacterial inactivation without the need of photo-activation. TiO_2-PET samples shown in Fig. 6, trace 8) reduced only marginally the bacteria. This shows again the drastic effect of Cu-decoration accelerating the bacterial inactivation even at Cu-levels of 0.08% (Table 1). Last, trace 9) shows the control run using PET under actinic light. No bacterial inactivation was found. Cu-ions reveal efficient antimicrobial activity

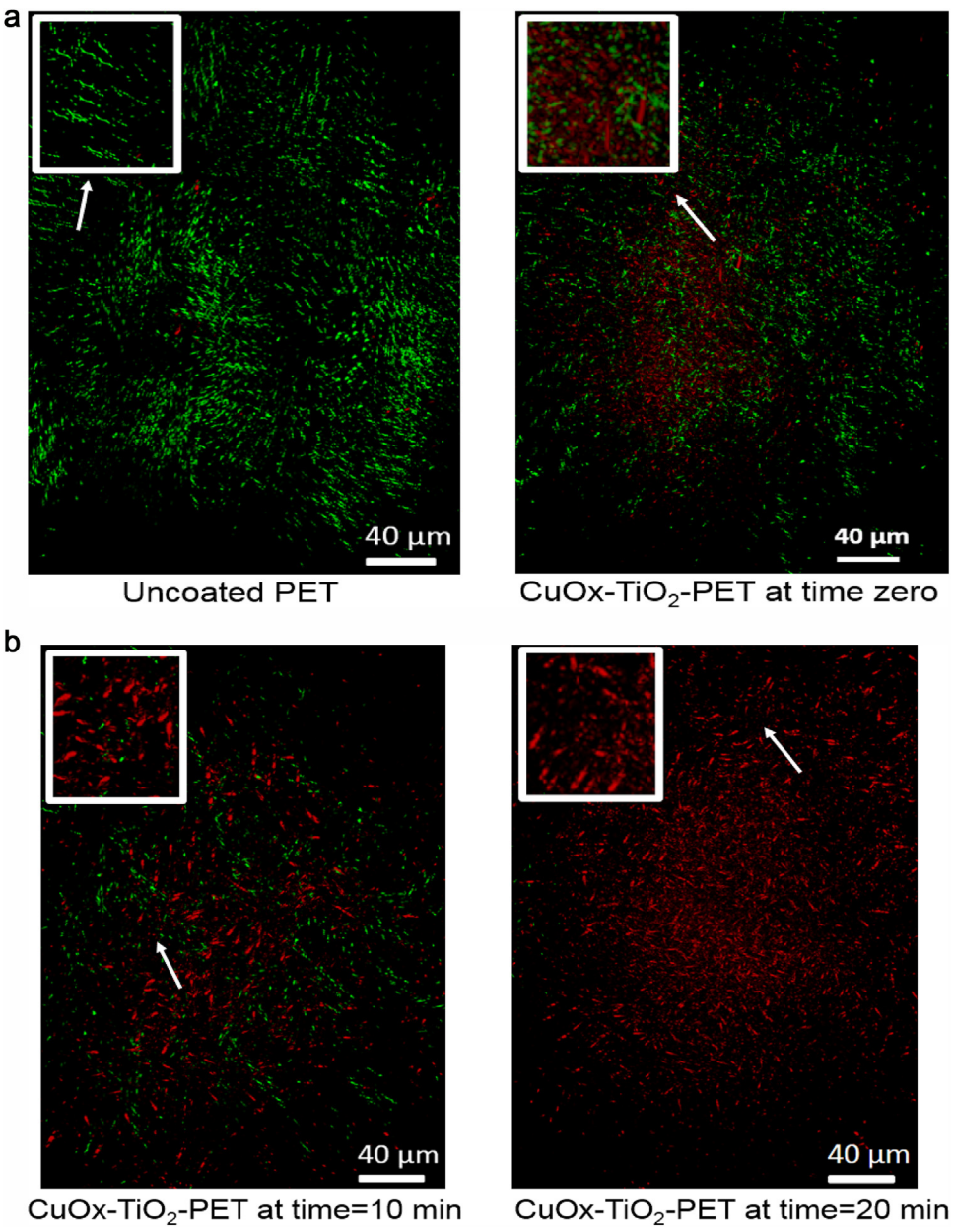

Fig. 7. a. Fluorescence stereomicroscopy of *E. coli* under low intensity actinic light showing the biofilm on: a) PET and b) on CuOx-TiO_2-PET samples at time zero (dark reaction). Green-dots refer to living cells and red-dots refer to dead cells. For other details see text. b. Biofilm inhibition on co-sputtered CuOx-TiO_2-PET samples after 10 and 20 min under 0.5 mW/cm^2 actinic light For other details see text.

degrading membrane/LPS layers [1,14,17,18,23,56]. Espirito-Santo [21,22] and Lemire et al. [57] have recently reported bacterial inactivation on Cu surfaces. Results presented in Fig. 6, traces 3) and 4) show that higher loadings of Cu did not lead to a faster bacterial inactivation kinetics due to their higher Cu-content, but that the bacterial inactivation was essentially due to Cu-ions. Some recent reports have addressed bacterial inactivation mediated by TiO_2 doped by N and S under light [58,59]. The faster bacterial inactivation kinetics induced by the co-sputtered CuOx-TiO_2-PET samples compared to N, S-doped TiO_2 is partly due to the effective binding of CuOx/TiO_2 with *E. coli*. The Cu(II)- species has been shown to be more susceptible to coordinate with proteins than N and S [1,2,18–20]. The bacterial inactivation by CuOx-TiO_2-PET within 20 min may preclude partially or completely the adhesion, aggregation and consequent spread of bacteria due to the biofilm formation. This is a crucial point important in the prevention of biofilm induced bacterial infection.

The release of Ti and Cu was monitored by inductive coupled plasma mass spectrometry (IPC-MS) and the results are presented in Table 2. Table 1 indicates an initial value for Ti 0.11%TiO_2 by weight on PE for the co-sputtered sample. This is a Ti-content equivalent to 1.1 10^5 µg Ti on a surface 2×2 cm PET. After the first bacterial inactivation cycle, the sample was digested with nitric acid 69% (1:1 $HNO_3 + H_2O$) to remove the organics in the solution and to insure that there were no adhered ions remaining on the flask wall. The samples droplets were introduced to the ICP-MS trough a peristaltic pump to the nebulizer. This allows the complete sample evaporation. The Ti and Cu found in the nebulizer droplets were subsequently quantified by mass spectrometry (MS). Table 2 reports a value of 9 ppb (or a concentration 9 micrograms) for the Ti. Dividing this value by the initial Ti-loading, the per cent loss can

Table 2
ICP-MS concentrations Ti and Cu-ions (ppb) released from co-sputtered TiO_2-Cu-PET (3 min) and sequentially sputtered TiO_2/Cu-PET (8 min/40 s) during bacterial inactivation cycles.

	First cycle		Third cycle		Fifth cycle	
	Ti	Cu	Ti	Cu	Ti	Cu
TiO_2-CuOx-PET co-sputtered for 3 min	9	5	6	4	6	4
TiO_2/CuOx-PET sequentially sputtered for 8 min/40 s	2	18	4	14	1	17

be estimated at <0.01%. In a similar way a value for the per cent loss of Cu can estimated of <0.01%. Very low ppb amounts of Ti and Cu were detected up to the 5th recycling. The Cu-release reported in Table 2 will not adversely affect the stable performance of the co-sputtered sample during long-term operation [60,61]. The amounts of Cu-ions in the ppb range by the co-sputtered and sequential sputtered Cu-samples reported in Table 2 are below the cytotoxic levels allowed for mammalian cells of 2–3 mg set by the World Health Organization (WHO) [62,63].

3.5. *Fluorescence stereomicroscopy monitoring of the bacterial inactivation*

Contrast phase and fluorescence microscopy analysis have been carried out to monitor the effect of the co-sputtered CuOx-TiO_2-PET on *E. coli*. Fig. 7a reports the fluorescence microscopy of the *E. coli* biofilm at time zero showing the green color of the cells preserving their initial celli wall integrity. The red color of the damaged cells appears instantly when the *E. coli* biofilm was contacted with the CuOx-TiO_2-PET sample. The density of the red dots due to the fluorchrome dye staining the bacteria DNA increased progressively at 10 and 20 min as shown in Fig. 7b. The last image taken at 20 min shows only red cells due to complete *E. coli* inactivation.

3.6. *X-Ray photoelectron spectroscopy (XPS) and evidence for redox catalysis*

The surface atomic concentration percentages for the co-sputtered and sequential sputtered catalysts are shown in Table 3. In both samples the amount of C increases after bacterial inactivation due to the deposition of the C-residues product of the bacterial decomposition. The O-surface enrichment is seen to decrease in the co-sputtered sample probably due to the increase in the C-content superimposing itself on the Ti, Cu-oxide layers after bacterial inactivation. The N- and Cu-contents is seen to remain fairly constant with time. N- comes from the bacterial inactivation and is rapidly destroyed on the sample surface. The Ti in the sequential sputtered sample increases after bacterial inactivation due to the C-residues collected on the sample surface within 90 min.

Fig. 8a and b shows the XPS spectra of the co-sputtered CuOx-TiO_2-PET and of the sequential sputtered CuOx/TiO_2-PET samples before and after bacterial inactivation. Fig. 8a show two Cu2pXPS peaks at 934.2 eV and 952.3 eV peaks attributed to Cu(II) before bacterial inactivation [44–46]. The symmetry of these peaks was not high due to the concomitant presence of small amounts Cu^0 and Cu(I) [57]. It is apparent that Cu(II) exists on the surface of the surface of the CuOx-TiO_2-PET sample coexisting with Cu(I) and Cu^{00}. After the 20 min disinfection (see Fig. 1) a small shift of these peaks to 934.7 eV and 953.9 eV was observed due to *redox* reactions on the sample surface interacting with bacteria.

Fig. 8b shows the peaks for the sequentially sputtered sample with Cu2p peaks at 932.5 eV and 952.3 eV before the disinfection period. These peaks shift to 934.2 eV and 954.3 eV after disinfection due to *redox* reactions of the Cu with bacteria. The two Cu2pXPS peaks at 932.5 eV and 952.3 eV are attributed to the Cu (I) doublet

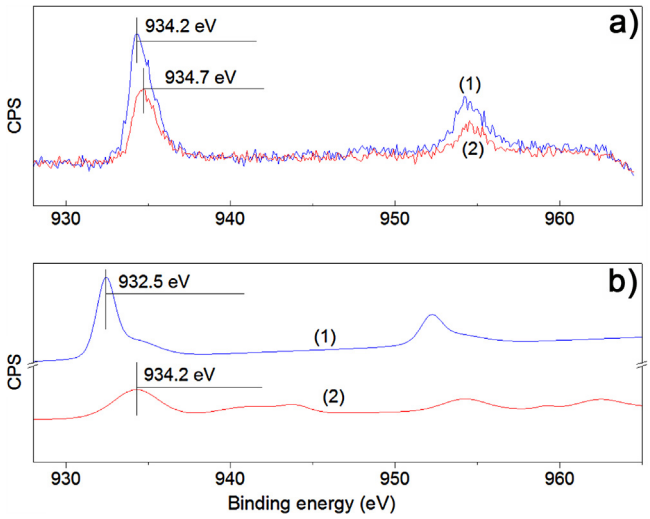

Fig. 8. a. XPS deconvolution of Cu2p in a CuOx-TiO_2-PET co-sputtered sample: (1) before and (2) after bacterial inactivation. b. XPS deconvolution of Cu2p in CuOx/TiO_2-PET sequentially sputtered sample: (1) before and (2) after bacterial inactivation.

Cu2p3/2 and 2Cu2p1/2 respectively [44,45]. The XPS results suggest the reactions

$$Cu^0 + O_2 \rightarrow 2Cu_2OE^0 0.41\,V \quad (1)$$

$$Cu^{2+} + Cu^0 + H_2O \rightarrow Cu_2O + 2H^+E^0 0.17\,V \quad (2)$$

$$2Cu_2O + O_2 \rightarrow 4CuOE^0 0.52\,V \quad (3)$$

The pattern of the Cu and Ti sputtered on PET is complicated by the surface diffusion controlling the mass transport of Cu (II)/Cu (I) and Ti on PET [58,59]. Fig. 9a present the etching on the co-sputtered sample applying 5 KeV Ar^+-ions. The etching of the Cu2pXPS doublet (934.2 eV and 952.3 eV) shows that the peaks of Cu(II) remain fairly constant up to 50 layers (10 nm). Next, Fig. 9b shows the Ti-peaks (Ti2p XPS doublet) within the first 0.6 nm from the topmost surface decreasing afterwards and remaining constant up to ~56 nm. The topmost layers of Cu and TiO_2 shown in Fig. 8a comprise multi-body catalysis intervening in the bacterial inactivation shown in Fig. 6 and this system could be more accurately discussed in the framework of the density functional theory [64].

Table 4 shows the changes in oxidation states for the sequentially sputtered and co-sputtered samples. The initial composition seen for the sequentially sputtered sample was Cu_2O (65.3%) decreasing to 24.7% after bacterial inactivation. For the co-sputtered samples (see right hand side of Table 4) CuO was determined at time zero (87%). This value decreased slightly to CuO (75.4%) due to reduction to Cu_2O occurring during bacterial inactivation. Different oxidation states of Cu/CuO lead to different bacterial inactivation kinetics (see Fig. 6). The XPS changes and bacterial inactivation kinetics induced by the co-sputtered and sequentially sputtered samples will be used to suggest a differentiated bacterial inactivation mechanism for both samples in the section below.

Table 3
Surface atomic percentage concentration determined by XPS for CuOx-TiO_2-PET co-sputtered and Cu/TiO_2 sequentially sputtered sample.

Sample		C	O	N	Cu	Ti
CuOx-TiO_2-PET co-sputtered for 3 min (sample contacted with bacteria)	Before bacterial loss of viability (time zero)	30.3	23.2	0.6	22	23.9
	After bacterial loss of viability (20 min)	36.5	18.7	0.9	20.8	23.1
TiO_2/CuOx-PET sequentially sputtered for 8 min/40 s (sample contacted with bacteria)	Before bacterial loss of viability (time zero)	33.9	16.4	1.1	38.6	10
	After bacterial loss of viability (90 min)	39.1	17	1.2	36.3	6.4

Table 4
Surface atomic percentage concentration of the Cu-species before, during and after total bacterial inactivation on sequentially sputtered CuOx/TiO_2-PET (10 min/40 s) and cosputtered CuOx-TiO_2-PET (3 min) samples.

Sample	Sequentially sputtered CuOx/TiO_2-PET		Co-sputtered CuOx-TiO_2 –PET	
	%Cu/Cu_2O	%CuO	%Cu/Cu_2O	%CuO
Time zero (sample non contacted with bacteria)	65.3	34.6	12.2	87.7
Time zero (sample contacted with bacteria for 1 min)	33.4	56.6	18.8	81.2
After total bacterial inactivation time (20 min) for the co-sputtered sample and (90 min) for sequentially sputtered sample.	24.7	75.2	24.6	75.4

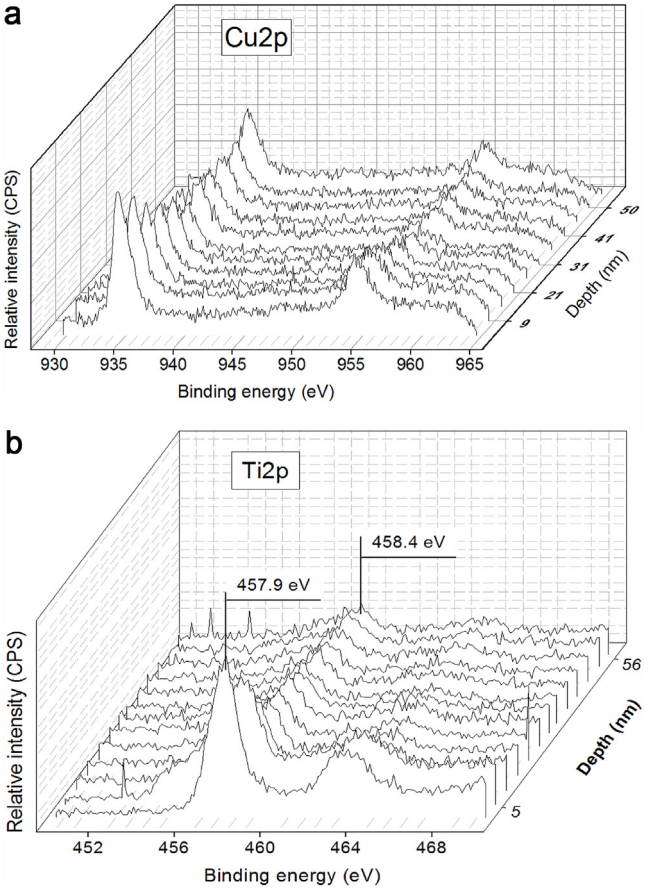

Fig. 9. a. 3D-XPS profile of the CuOx topmost Cu2p layers in the co-sputtered CuOx-TiO_2-PET sample before bacterial inactivation. b. 3D-XPS of the TiO_2 topmost Ti2p layers in the co-sputtered CuOx-TiO_2-PET sample before bacterial inactivation.

3.7. Mechanism suggested for the vectorial charge transfer on co-sputtered and sequentially sputtered samples

Recently interfacial charge transfer (IFCT) was reported under solar light (UV–vis) for a sputtered CuOx/TiO_2 catalyst [34,35]. By XPS the CuO was identified as being the main species on the co-sputtered catalyst (CuOx-TiO_2-PET). The IFCT rate is determined by the position of the relative potential energy levels (but not only) of the TiO_2 and CuO-bands. The distinct bacterial inactivation times induced by the two samples are a function of the conduction band (cb) and valence band (vb) positions of CuO and Cu_2O. The vectorial charge-transfer for both samples is shown in Fig. 10a/b. The CuO presents a band-gap (of 1.7 eV), cb (−0.3 eV) and vb (+1.7 eV), while direct band-gap of Cu_2O (p-type) presents a band-gap of (2.1 eV), cb (−1.4 eV) and vb (+0.6 eV) [31–33].

The higher efficiency by the co-sputtered (CuOx-TiO_2-PET) containing mainly CuO can be rationalized by the effect of the TiO_2 suppressing the recombination of the photo-generated cb(e−)/vbh(+) in the CuO-TiO_2. Cu_2O absent in the XPS-spectrogram reported in Fig. 8a. In air atmosphere Cu_2O gets covered by layers of CuO [65]. The co-sputtered catalyst in Fig. 10a shows hat the electron injection from CuO to TiO_2 is thermodynamically feasible. The electrons generated by the TiO_2 will be trapped by Cu^{2+}, and reduce the Cu^{2+} to Cu^+ (Cu_2O). Subsequently, Cu-oxide reacts with O_2(air) leading to the formation of CuO as shown Eq. (4)

$$CuO + e- \rightarrow Cu_2O + O_2(air) \rightarrow CuO \quad (4)$$

Furthermore, the fast reactions of Cu^+ and Cu^0 with O_2(air) will hinder the cbe−/vbh+ recombination as shown by Eqs. (5) and (6) below:

$$Cu^+ + O_{ads} \rightarrow Cu^{2+} + O^-_{ads} \quad (5)$$

$$Cu + O_{ads} \rightarrow Cu^+ + O^-_{ads} \quad (6)$$

In the sequential sputtered catalyst, the high absorption coefficient of Cu_2O and the low diffusion length of the minority carrier was reported to lead to a low photo-efficiency in the Cu_2O (p-type) semiconductor [66,67].

3.8. Mechanism suggested for the bacterial inactivation on co-sputtered (CuO) and sequentially sputtered (Cu_2O) samples

Since the photocatalytic mechanism of TiO_2 has been widely reviewed [1,18,28], we suggest hereby the mechanistic steps for the co-sputtered catalyst in agreement with reference [68] (Fig. 10a):

$$CuO + h\nu \rightarrow CuO(cbe-) + CuO(vbh+) \quad (7)$$

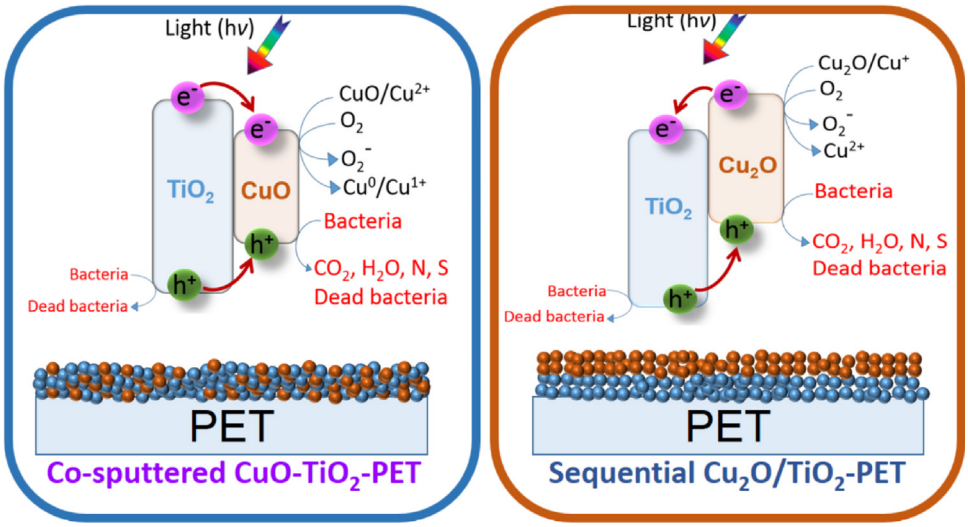

Fig. 10. a. Mechanism suggested for the antibacterial activity of co-sputtered CuO-TiO_2-PET on *E. coli.* b. Mechanism suggested for antibacterial activity of sequentially sputtered Cu_2O/TiO_2-PET on *E. coli.*

Under photon energies exceeding the CuO band-gap, the cbe- electron react directly with the O_2 forming O_2^- Eq. (3) or reduce the Cu^{2+} to Cu^+ as noted in Eqs. (9)–(11):

$$CuO(cbe-) + O_2 \rightarrow CuO + O_2^- \quad (8)$$

$$CuO(cbe-) \rightarrow CuO(Cu^+) \quad (9)$$

$$CuO(Cu^+) + O_2 \rightarrow CuO(Cu^{2+}) + O_2^- \quad (10)$$

$$CuO(Cu^+) \rightarrow CuO_{vacancy} + Cu^+ \quad (11)$$

For the sequentially CuOx/TiO_2-PET sputtered catalyst under light the reactions can be suggested below by Eqs. (12)–(15). The highly mobile electrons transfer from Cu_2Ocb to the TiO_2cb as noted in Eq. (13) and Fig. 10b. The vbh+ reacts oxidizing bacteria.

$$Cu_2O + h\nu \rightarrow Cu_2O(cbe-), Cu_2O(vbh+) \quad (12)$$

$$Cu_2O(cbe-) + TiO_2 \rightarrow TiO_2{}^-or(Ti^{3+}) + Cu_2O \quad (13)$$

$$TiO_2{}^- + O_2 \rightarrow TiO_2 + O_2^- \quad (14)$$

$$Cu_2O(vbh+) + bactéria \rightarrow (CO_2, H_2O, inorg.N, S) + Cu_2O \quad (15)$$

4. Conclusions

This work presents the first quantitative evidence for the effect of different atomic-scale microstructure of Cu-Ti composite catalysts on the bacterial inactivation kinetics. The roughness, optical absorption, nanoparticle distribution, coating thickness and the atomic percentage concentration were identified for the co-sputtered and sequential sputtered catalysts. The catalysts investigated presented an almost equal low Cu and Ti atomic per cent loading on the polyethylene (PET) substrate. In the co-sputtered and sequential sputtered catalysts, the presence of CuOx induced a red shift with respect to the UV–vis absorption of TiO_2 allowing the absorption of visible/solar light radiation. The superior activity of the co-sputtered CuOx-TiO_2-PET catalyst seems to be based on the high loading of CuO compared to the sequential sputtered CuOx/TiO_2-PET. The later composite was observed to be richer in Cu_2O. The mechanism of charge transfer mechanism (IFCT) was suggested for both catalyst samples. Femtosecond spectroscopy was used to follow the transient absorption and electron injection by light excitation. At least three transients were detected by the classical pump-probe approach in the fs-ps domain.

Acknowledgments

We thank the EPFL, the Swiss National Science Foundation (SNF) Project No 200021-143283/1 and Russian Foundation for Basic Research grant: RFBR 14-03-00546 for financial support.

Appendix A. Supplementary data

Supplementary data associated with this article can be found, in the online version, at http://dx.doi.org/10.1016/j.apcatb.2017.02.043.

References

[1] J.A. Byrne, P.S.M. Dunlop, J.W.J. Hamilton, P. Fernández-Ibáñez, I. Polo-López, P. Kumar Sharma, A.S.M. Vennard, A review of heterogeneous photocatalysis for water and surface disinfection, Molecules 20 (2015) 5574–5615.
[2] D. Canpoccia, L. Montanaro, C.R. Arciola, A review of the biomaterials technologies for infection resistant surfaces, Biomaterials 34 (2013) 8533–8554.
[3] D. Sun, M.B. Shahzad, M. Li, G. Wang, D. Xu, Antimicrobial materials with medical applications, Mater. Technol. Adv. Perform. Mater. 30 (2015) B90–95.
[4] I. Francolini, G. Donelli, Prevention and control of biofilm-based medical device-related infections, FEMS Immunol. Med. Microbiol. 59 (2010) 227–238.
[5] H. Foster, I. Ditta, S. Varghese, A. Steele, Photocatalytic disinfection using titanium dioxide: spectrum and mechanics of antimicrobial activity, Appl. Microb. Biotechnol. 90 (2011) 1847–1868.
[6] R.M. Klevens, J.R. Edwards, C.L. Richards Jr., T.C. Horan, R.P. Gaynes, D.A. Pollock, D.M. Cardo, Estimating health care-associated infections and deaths in U. S. hospitals, 2002, Public Health Rep. 122 (2007) 160–166, Washington DC.
[7] J.N. Anderl, M.J. Franklin, P.S. Stewart, Role of antibiotic penetration limitation in *Klebsiella pneumonaie* biofilm resistance to ampicillin and ciprofloxacin, Antomicrob. Agents Chemother. 44 (2000) 1818–1824.
[8] K. Taylor, J. Roberts, The Challenge of Hospital Acquired Infections (HAI), Nat. Audit Office., 2002.
[9] D. Talon, The role of the hospital environment in the epidemiology of multi-resistant bacteria, J Hosp. Infect. 43 (1999) 13–17.
[10] A. Kramer, I. Schwebke, G. Kampf, How long do nosocomial pathogens persist on inanimate surfaces? A systematic review, BMC Infect. Dis. 6 (2006) 130–139.
[11] K. Sunada, T. Watanabe, K. Hashimoto, Bactericidal activity of copper-deposited TiO_2 films under weak UV-light illumination, Environ. Sci. Technol. 37 (2003) 4785–4789.
[12] H. Irie, K. Kamiya, T. Shibanuma, Sh. Miura, D. Tryk, T. Yo koyama, K. Hashimoto, Visible light sensitive Cu(II)-grafted TiO_2 photocatalysts: activities and X-ray absorption fine structure analyses, J. Phys. Chem. C 113 (2009) 10671–10766.
[13] H. Irie, Sh. Miura, K. Kamiya, K. Hashimoto, Efficient visible light-sensitive photocatalysts: grafting Cu(II) onto TiO_2 and WO_3 photocatalysts, Chem. Phys. Lett. 457 (2008) 202–205.

[14] X. Qiu, M. Miyauchi, K. Sunada, M. Minoshima, M. Liu, Y. Lu, M. Ding, Y. Shomodara, Y. Hosogi, Y. Kuroda, K. Hashimoto, Hybrid Cu_x/TiO_2 nanocomposites as risk-reduction materials in indoor environments, ACS Nano 6 (2012) 1609–1618.
[15] P. Evans, D. Sheel, Photoactive and antibacterial thin films on stainless steel, Surf. Coat. Technol. 201 (2007) 9319–9324.
[16] H.A. Foster, D.W. Sheel, P. Shel, P. Evans, S. Varghese, N. Rutschke, M.H. Yates, Antimicrobial activity of titania/silver and titania/copper films prepared by CVD, J. Photochem. Photobiol. A 216 (2010) 283–289.
[17] M.H. Yates, L.A. Brook, B.I. Ditta, P. Evans, H.A. Foster, W.D. Sheel, A. Steele, Photo-induced self-cleaning and biocidal bahavior of titania and copper oxide multiilayers, J. Photochem. Photoboiol. A 197 (2008) 197–205.
[18] V. Etacheri, C. Di Valentin, D. Schneider, D. Bahnemann, S. Pillai, Visible-light activation of TiO_2 photocatalysts: advances in theory and experiments, J. Photochem. Photobiol. C Rev. 25 (2015) 1–29.
[19] R. Fagan, Mc. Cormack, D. Dionysiou, S. Pillai, A review on solar and visible light active TiO_2 photocatalysts for treating bacteria, cynotoxins and contaminants of emerging concern, Mater. Sci. Semicond. Process. 42 (2016) 2–14.
[20] N. Leyland, A. Podporska, J. Caroll, J. Browne, S. Hinder, B. Quilty, S. Pillai, Highly efficient F, Cu-doped TiO_2 antibacterial visible light active photocatalytic coatings to combat hospital acquired infections, Nat. Sci. Rep. (2016) 6, Article 24770.
[21] D. Quaranta, T. Krans, C. Espirito Santo, C. Elowsky, D. Domaille, C. Chang, G. Grass, Mechanisms of contact-mediated killing of yeast cells on dry metallic copper surfaces, Appl. Environ. Microbiol. 77 (2011) 416–4126.
[22] C. Espirito Santo, E. Lam, C. Elowsky, D. Quaranta, D. Domaille, C. Chang, G. Grass, Bacterial killing by dry metallic copper surfaces, Appl. Environ. Microbiol. 77 (2011) 794–802.
[23] G. Borkow, J. Gabbay, Putting copper into action: copper impregnated products with potential biocidal activities, J. FASEB (2008) 1728–1730.
[24] G. Borkow, J. Gabbay, Copper an ancient remedy returning to fight microbial, fungal and viral infections, Curr. Chem. Biol. 3 (2009) 272–278.
[25] R. Liu, K. Memarzadeh, B. Zhang, Y. Zhang, Z. Ma, R. Allaker, L. Ren, K. Yang, Antibacterial effect of copper bearing titanium alloy (Ti-Cu) against *Streptococcus mutans and Porphyromonas gingivalis*, Nat. Sci. Rep. 6 (2016) 29885–29995.
[26] M. Pelaez, T. Nolan, S. Pillai, K. Seery, P. Falaras, A. Kontos, P.S.M. Dunlop, J. Hamilton, J.-A. Byrne, K. O'Shea, M. Entezari, D. Dionysiou, A review on the visible light active titanium dioxide photocatalysts for environmental applications, Appl. Catal. B 125 (2012) 331–349.
[27] S. Banerjee, S. Pillai, P. Falaras, K. O'Shea, A.-J. Byrne, D. Dionysiou, New insights into the mechanism of visible light photocatalysis, J. Phys. Chem. Lett. 5 (2014) 2543–2554.
[28] J. Schneider, M. Matsuoka, J. Takeuchi, L. Zhang, Y. Horiuchi, M. Anpo, D. Bahnemann, Understanding TiO_2 photocatalysis: mechanisms and materials, Chem. Rev. 114 (2014) 9919–9986.
[29] J. Huang, S. Wang, Y. Zhao, X. Wang, S. Wang, S. Wu, S. Zhang, W. Huang, Synthesis and characterization of CuO/TiO_2 catalysts for low-temperature CO oxidation, Catal. Commun. 7 (2006) 1029–1034.
[30] Y. Wu, F. Li, H. Wang, E. Alarousu, Y. Chen, B. Lin, L. Wang, M. Hedhili, Y. Li, K. Wu, X. Wang, O. Mohammed, T. Wu, Ultrathin CuO as an efficient inorganic hole transporting material for perovskite solar cells, Nanoscale 8 (2016) 6173–6179.
[31] A. Briskman, Study of electrodeposited Cu_2O photovoltaic cells, Sol. Energy Mater. Sol. Cells 27 (1992) 361–368.
[32] A. Nozik, Photo-electrochemistry: applications to solar energy conversion, Ann. Rev. Phys. Chem. 189 (1978) 521–549.
[33] J. Kiwi, C. Morrison, Heterogeneous photocatalysis: dynamics of charge transfer in Li-doped anatase based catalyst powders with enhanced water photocleavage under UV-radiation, J. Phys. Chem. 88 (1984) 6146–6152.
[34] S. Rtimi, R. Sanjines, C. Pulgarin, J. Kiwi, Accelerated *Esherichia coli* inactivation in the dark on uniform copper flexible surfaces, Biointerphases 9 (2) (2014) 029012.
[35] S. Rtimi, O. Baghriche, C. Pulgarin, J.-C. Lavanchy, J. Kiwi, Growth of TiO_2/Cu by HIPIMS for accelerated bacterial loss of viability, Surf. Coat. Technol. 232 (2013) 804–813.
[36] S. Rtimi, C. Pulgarin, R. Sanjines, V. Nadtochenko, J.-C. Lavanchy, J. Kiwi, Preparation and mechanism of Cu-decorated TiO_2-ZrO_2 films showing accelerated bacterial inactivation, ACS Appl. Mater. Interfaces 7 (2015) 12832–12839.
[37] S. Rtimi, C. Pulgarin, M. Bensimon, J. Kiwi, New evidence for Cu decorated binary-oxides mediating the bacterial inactivation/mineralization in aerobic media, Colloids Surf. B: Bio-Interfaces 144 (2016) 222–228.
[38] T. Cushnie, P. Robertson, S. Officer, M. Pollard, R. Prabhu, C. McCullagh, C. Robertson, Photobacterial effects of TiO_2 thin films at low temperatures: a primary study, J. Photochem. Photobiol. A 216 (2010) 290–294.
[39] N.L. Dias, Adsorption of Cu(II) and Co(II) complexes on a silica gel surface chemically modified with 2-mercaptoimidazole, Mikrochim. Acta 130 (1999) 233–240.
[40] M. Mejia, M. Marin, G. Restrepo, C. Pulgatin, E. Mielczarski, J. Mielczarski, Y. Arroyo, J.-C. Lavanchy, J. Kiwi, J Self-cleaning modified TiO_2-cotton by UVC-light (185 nm) and RF-plasma in vacuum and under atmospheric pressure, Appl. Catal. B 91 (2009) 481–488.
[41] S. Rtimi, C. Pulgarin, V. Nadtochenko, F. Gostev, I. Shelaev, J. Kiwi, FeOx-TiO_2 film with different microstructures leading to femtosecond transients with different properties: biological implications under visible light, Sci. Rep. 6 (2016) 30113–30123.
[42] A.R. Smith, Semiconductors, 2nd ed., Cambridge Univ press, Cambridge, UK, 1979.
[43] J. Andrews, V. Hitelman, in: B. Di Bartolo (Ed.), Spectroscopy of Solid State Laser Materials, Plenum Press, N.Y. USA, 1987, p. 513.
[44] C.D. Wagner, W.M. Riggs, L.E. Davis, F.G. Moulder, E. Mullenberg, Handbook of X-ray Photoelectron Spectroscopy, 2nd ed., 1979, Minn, USA.
[45] J. Nogier, M. Delamar, P. Ruiz, P. Albers, J. Kiwi, XPS and SIMS characterization, Catal. Today 56 (2000) 403–413.
[46] D.A. Shirley, High-resolution X-ray photoemission spectrum of the valence bands of gold, Phys. Rev. B 5 (1972) 4709–4714.
[47] S.A. Kovalenko, A.L. Dobryakoc, J. Ruthman, N.P. Ernsting, Femtosecond spectroscopy of condenses phases with chirped supercontinuum probing, Phys Rev. A 59 (1999) 2369–2384.
[48] Yu E. Lozovic, A.L. Dobryakoc, N.P. Ernsting, S.A. Kovalenko, New method of non-fermi liquid study by pump-supercontinuum probe femtosecond spectroscopy, Phys. Lett. A 223 (1996) 303–307.
[49] Benjamin Gilbert, Jordan E. Katz, Nils Huse, Xiaoyi Zhang, Cathrine Frandsen, Roger W. Falcone, Glenn A. Waychunas, Ultrafast electron and energy transfer in dye-sensitized iron oxide and oxyhydroxide nanoparticles, Phys. Chem. Chem. Phys. 15 (2013) 17303–17313.
[50] J. Cherepy, N. Smested, M. Gratzel, Z. Zhang, Ultrafast electron injection: implications for a photo-electrochemical cell utilizing an anthocyanin dye sensitized TiO_2 nanocrystalline electrode, J. Phys. Chem. B 101 (1997) 9342–9351.
[51] C. Fitzmorris, M. Patete, J. Smith, X. Mascorro, S. Adams, S. Wong, I. Zhang, Ultrafast transient absorption studies on hematite nanoparticles the effect of particle shape on exciton dynamics, ChemSusChem 6 (2013) 1907–1912.
[52] S. Pendlebury, X. Wang, F. Le Formal, M. Cornuz, A. Kafizas, S. Tilley, M. Gratzel, J. Durrant, Ultrafast charge carrier recombination and trapping in hematite photoanodes under applied bias, J. Am. Chem. Soc. 136 (2014) 9854–9859.
[53] D. Wheeler, G. Wang, Y. Ling, Y. Li, J. Zhang, Nanostructured hematite: synthesis, characterization, charge carrier dynamics and photo-electrochemical properties, Energy Environ. Sci. 5 (2012) 6682–6702.
[54] Y. Jeyachandran, S. Narayandass, The effect of thickness of titanium nitride coatings on bacterial adhesion, Trends Biomater. Artif. Org. 24 (2010) 90–93.
[55] V. Nadtochenko, A. Rincon, S. Stanka, J. Kiwi, Dynamics of E coli photokilling due to cell wall lysis during TiO_2 photocatalysis, J. Photochem. Photobiol. A 169 (2005) 131–137.
[56] S. Robin, T. Soulimane, S. Lavelle, Interactions of biofilm-forming bacteria with abiotic surfaces, in: S.A.M. Tofail (Ed.), RSC Nanoscience and Nanotechnology No 21, Biological Interactions with Surface Charges in Biomaterials, 2012, RSC.
[57] A. Lemire, J. Harrison, J. Turner, Antimicrobial activity of metals: mechanisms, molecular targets and applications, Nat. Rev. Microbiol. 11 (2013) 371–384.
[58] R. Bacsa, J. Kiwi, T. Ohno, P. Albers, V. Nadtochenko, Preparation, testing and characterization of doped TiO_2 able to transform biomolecules under visible light irradiation by peroxidation/oxidation, J. Phys. Chem. B 109 (2005) 5994–6003.
[59] A.J. Rengifo-Herrera, K. Pierzchala, A. Sienkiewicz, L. Forro, J. Kiwi, J. Moser, C. Pulgarin, New evidence for the nature of the N, S do-doped TO_2 under visible light leading to *E. coli* inactivation: catalyst characterization, J. Phys. Chem. C 114 (2010) 2717–2723.
[60] S. Rtimi, R. Sanjines, C. Pulgarin, M. Bensimon, J. Kiwi, Insight on the photocatalytic bacterial inactivation by co-sputtered TiO_2-Cu in aerobic and anaerobic conditions, Appl. Catal. B 182 (2016) 277–285.
[61] L. Mei, M. Zheng, Z. Ye, Towards a molecular understanding of the antibacterial mechanism of copper-bearing titanium alloys against staphylococcus aureus, Adv. Healthc. Mater. 5 (2015) 557–566.
[62] I. Burghardt, F. Luthen, C. Prinz, B. Kreikemeyer, C. Zietz, H.G. Neumann, J. Rychly, A dual function of Copper in designing regenerative implants, Biomaterials 44 (2015) 36–44.
[63] ISO-10993-5: Biological Evaluation of Medical Device, Part 5: Test in Vitro for Cytotoxicity in Vitro Methods, ANSI-AAMI, Arlington VA, 2009.
[64] W. Kohn, Electronic structure of matter-wave functions and density functionalities, Rev. Mod. Phys. 71 (1999) 1253–1266.
[65] H. Zhang, C. Shen, S. Chen, Z. Xu, F. Liu, J. Li, H. Gao, Morphologies and microstructures of nano-sized Cu_2O particles using acetyl-trimethylammonium template, Nanotechnology 16 (2005) 267–272.
[66] A. Mittiga, E. Salza, F. Sartzo, M. Tucci, R. Vasanthi, Heterojunction Solar cells with 2% efficiency based on a Cu_2O substrate, Appl. Phys. Lett. 88 (2006) 163502.
[67] A. Noguet, D. Pierrat, M. Tapero, P. Zielinger, Longueur de diffusion des porteurs minoritaires et structure de jonction des diodes Cu/Cu_2O, J. Rev. Phys. Appl. (Paris) 15 (1980) 595–602.
[68] L. Yoong, F. Chong, B. Kutta, Development of copper-doped TiO_2 photocatalyst for hydrogen production under visible light, Energy 34 (2009) 1652–1661.